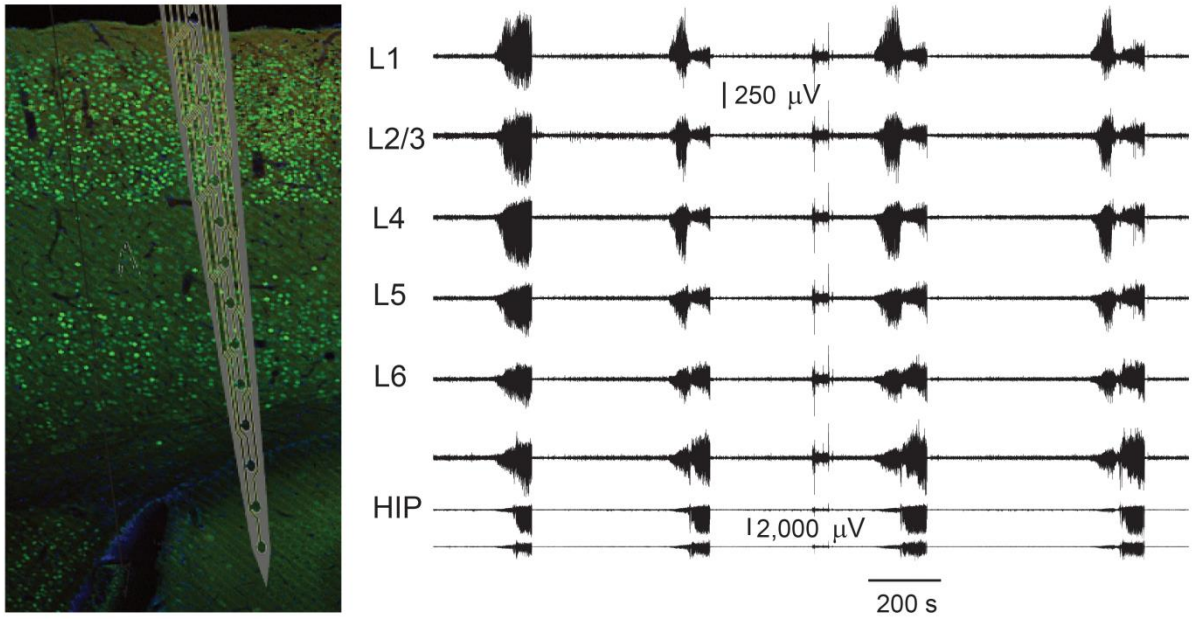

Supplementary Figure 1 Experimental setup of 16-channels silicone probe recordings from somatosensory cortex of P15 *Tsc1*$^{+/-}$ mouse. Left: CUX1 staining is used to identify L1-L4 cortical layers. Right: Example of the intracortical EEG recordings in head-restrained P15 *Tsc1*$^{+/-}$ mouse without any pharmacological treatment. Shown are epileptic discharges recorded at the layers indicated on the left of each trace. HIP-hippocampus.

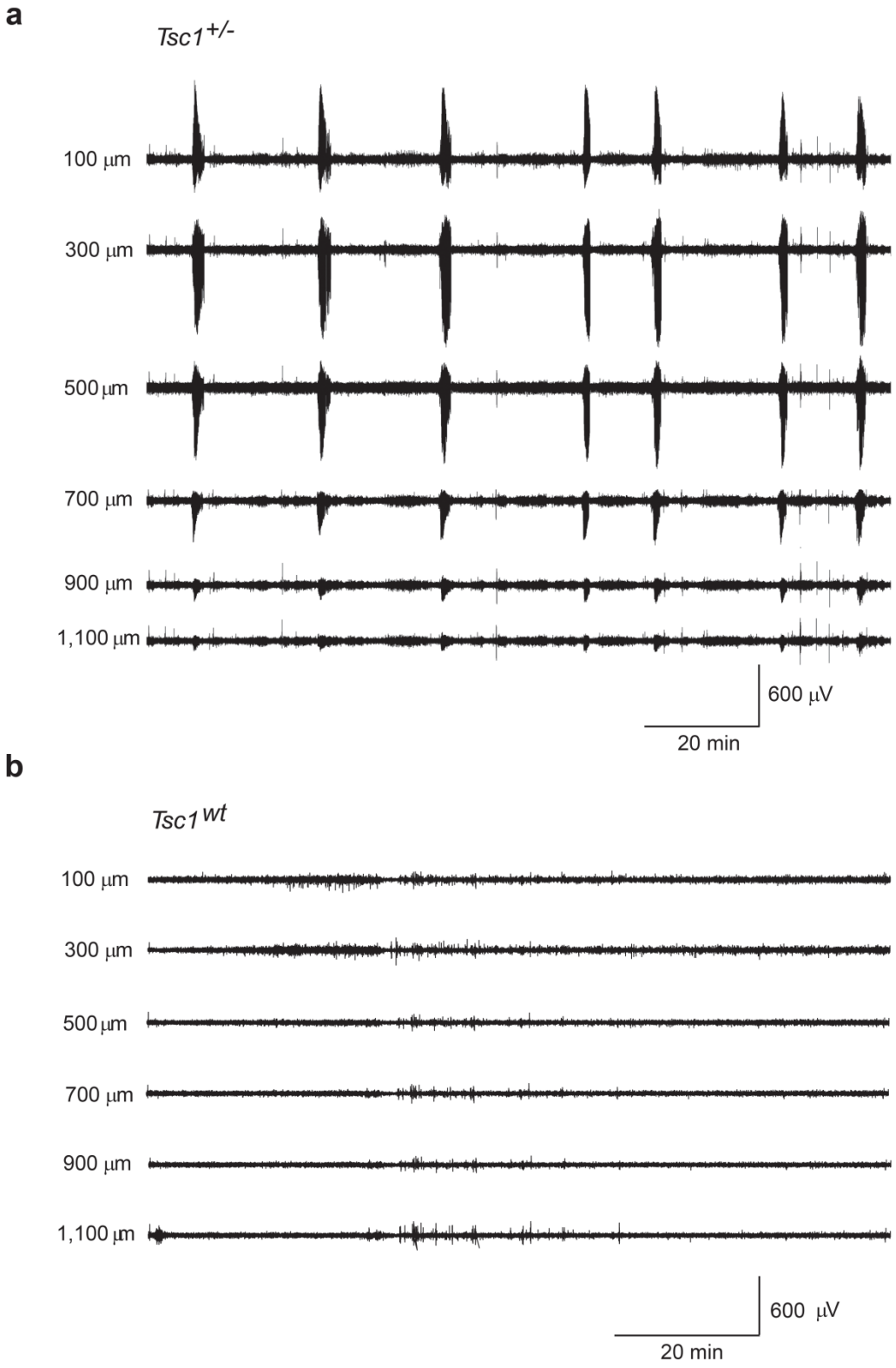

Supplementary Figure 2 Spontaneous seizures in *Tsc1*$^{+/-}$ mice. (**a**) Example of the 2 hours-long intracortical EEG recordings in head-restrained P15 *Tsc1*$^{+/-}$ mouse without any pharmacological treatment. The upper trace corresponds to the superficial electrode placed at 100 μm from the pia. Shown are epileptic discharges recorded at the depths indicated on the left of each trace. (**b**) Example of the intracortical EEG recordings in head-restrained P15 litter-mate *Tsc1*^{wt} mouse. Shown are traces recorded at the depths indicated on the left of each trace.

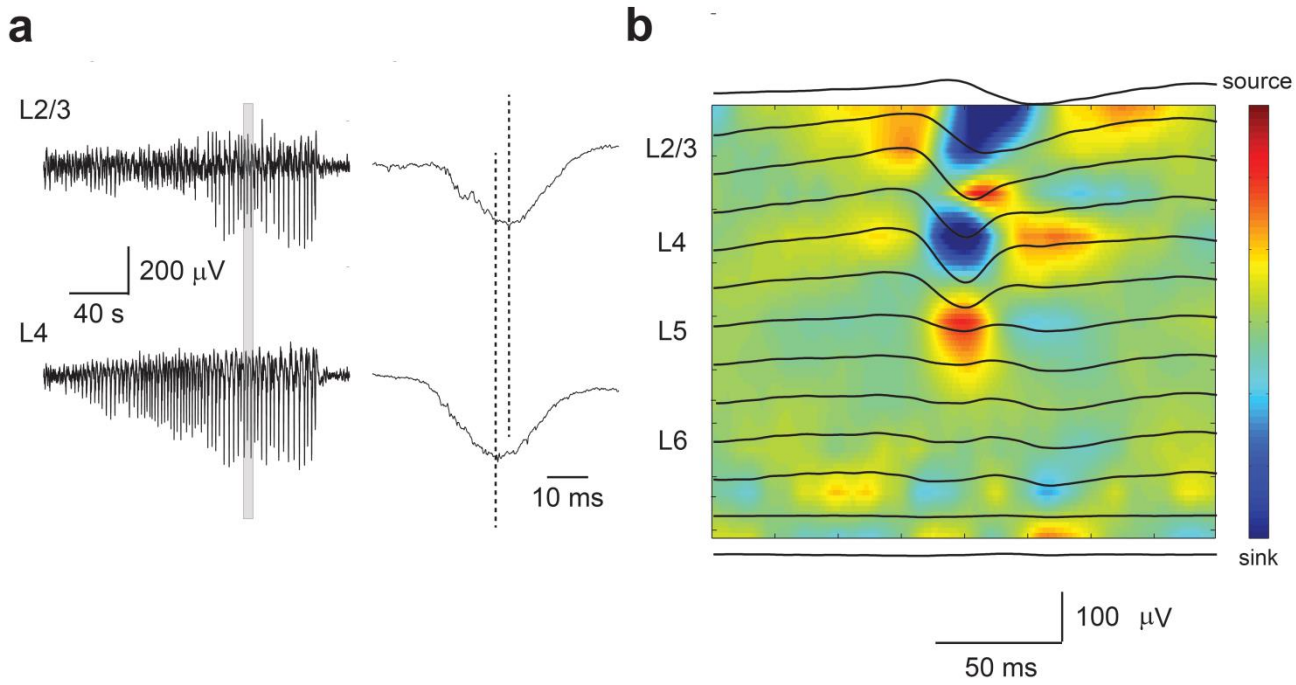

Supplementary Figure 3 Seizure onset in L4 preceded that in higher and lower neocortical layers. (**a**) Left: Representative electrographic seizures in L2/3 and L4 of neocortex Right: Expanded traces of the same seizures marked by grey box. Vertical dotted lines outline respective peaks. (**b**) Averaged population spikes at different cortical depths (black traces) superimposed with the corresponding current source density (CSD) map (n=29 population spikes).

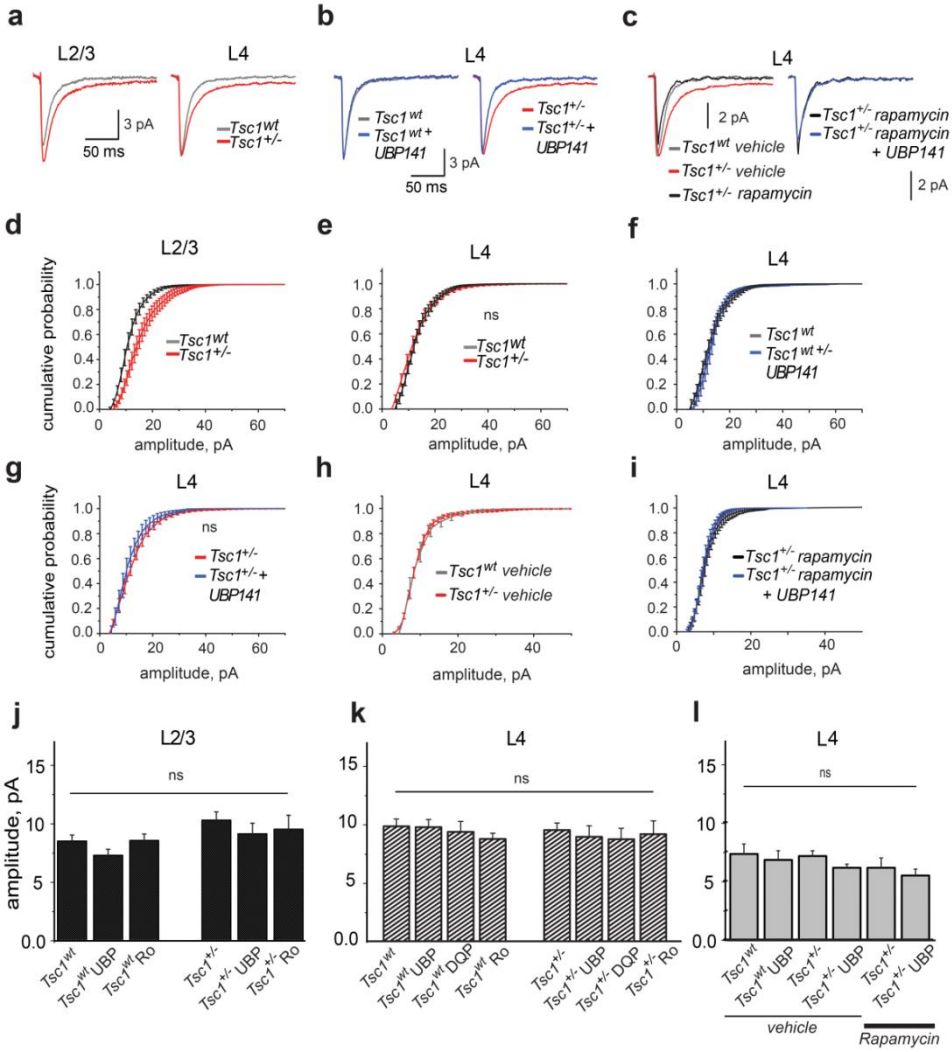

Supplementary Figure 4 Comparison of sEPSC amplitudes in *Tsc1*$^{+/-}$ and *Tsc1*^{wt} mice. (**a**) Superimposed grand average traces of sEPSC recorded from pyramidal neurons in L2/3 (left) or spiny stellate cells in L4 (right) of *Tsc1*^{wt} and *Tsc1*$^{+/-}$ mice at -50 mV. For each neuron original traces from individual experiments were aligned based on the starts of their rising phases and averaged. These averaged traces from individual experiments were averaged to form grand average traces shown. Pooled data from 16 neurons for *Tsc1*^{wt} and 27 neurons for *Tsc1*$^{+/-}$ in L2/3 and from 29 neurons for *Tsc1*^{wt} and 34 neurons for *Tsc1*$^{+/-}$ in L4. (**b**) Superimposed grand average traces of sEPSC recorded in L4 in *Tsc1*^{wt} and *Tsc1*$^{+/-}$ mice in control and in the presence of 10 μM UBP141. (**c**) Superimposed grand average traces of sEPSC recorded in L4 in *Tsc1*$^{+/-}$ and *Tsc1*^{wt} mice pretreated with either vehicle or rapamycin in control and in the presence of 10 μM UBP141. (**d, e**) Cumulative probabilities of amplitudes of sEPSCs recorded in *Tsc1*^{wt} (n=16, N=5 mice) and *Tsc1*$^{+/-}$ mice (n=27, N=8) in L2/3 (**d**) and in *Tsc1*^{wt} (n=18, N=5) and *Tsc1*$^{+/-}$ mice (n=34, N=10) in L4 (**e**). (**f, g**) Cumulative probabilities of amplitudes of sEPSCs recorded in L4 in control and in the presence of 10 μM UBP141 in *Tsc1*^{wt} (n=10, N=3) (**f**) and *Tsc1*$^{+/-}$ (**g**) mice. (**h**) Cumulative probabilities of amplitudes of sEPSCs recorded in L4 in *Tsc1*$^{+/-}$ (n=11, N=3) and *Tsc1*^{wt} mice (n=12, N=3) pretreated with vehicle. (**i**) Cumulative probabilities of amplitudes of sEPSCs recorded in L4 in *Tsc1*$^{+/-}$ mice pretreated with rapamycin in control (n=15, N=3) and in the presence of 10 μM UBP141 (n=11, N=3). For pairs of cumulative probabilities shown in (**e-i**) distributions do not differ significantly (Mann-Whitney test: p>0.05). For pair shown in (**d**) distributions differ significantly Mann-Whitney test: p<0.05. (**j**) Summary data for the effects of UBP141 (10 μM) and Ro25-6981 (1 μM) on amplitudes of sEPSC in L2/3 in *Tsc1*^{wt} and in *Tsc1*$^{+/-}$ mice. (**k**) Summary data for the effects of UBP141 (10 μM), DQP1105 (10 μM) and Ro25-6981 (1 μM) on amplitudes of sEPSC in L4 in *Tsc1*^{wt} and in *Tsc1*$^{+/-}$ mice. (**l**) Summary data for the effects of UBP141 (10 μM) on amplitude of sEPSC in L4 in *Tsc1*^{wt} and in *Tsc1*$^{+/-}$ mice pretreated with either vehicle or rapamycin. All data sets were analyzed using one-way ANOVA (see **Supplementary Table 2** for statistics). Error bars:±s.e.m.

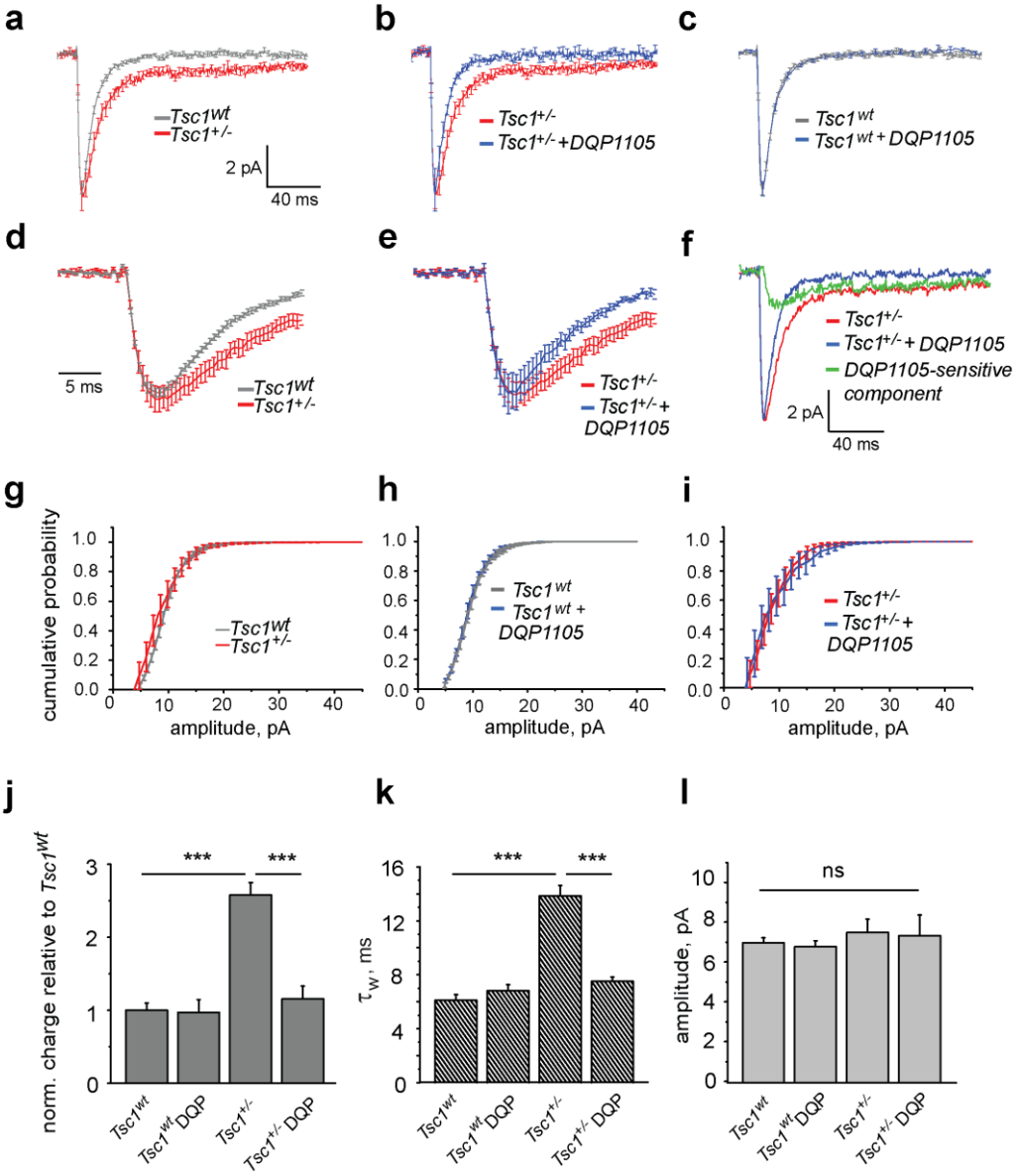

Supplementary Figure 5 Functional up-regulation of GluN2C/D subunits containing NMDA receptors in *Tsc1*$^{+/-}$ mice revealed by mEPSC recordings in L4 spiny stellate cells. (**a,d**) Superimposed grand average traces of mEPSC recorded in *Tsc1*^{wt} and *Tsc1*$^{+/-}$ mice at -50 mV. Error bars on panels (**a,b,d,e**): ±s.e.m. Panel (**d**) shows the same traces as in (**a**) at expanded time scale. Pooled data from 8 - 10 neurons, N=3 mice for each group. (**b,e**) Superimposed grand average traces of mEPSC recorded in *Tsc1*$^{+/-}$ mice in control and in the presence of 10 μM DQP1105. Panel (**e**) shows the same traces as in (**a**) at expanded time scale. (**c**) Superimposed grand average traces of mEPSC recorded in *Tsc1*^{wt} mice in control and in the presence of 10 μM DQP1105. (**f**) DQP-sensitive mEPSC component in *Tsc1*$^{+/-}$ mice (green trace) revealed by subtraction of the trace with DQP1105 (blue) from the trace without DQP1105 (red). (**g**) Cumulative probabilities of amplitudes of mEPSCs recorded in *Tsc1*^{wt} (n=9, N=3) and *Tsc1*$^{+/-}$ (n=10, N=3) mice. (**h,i**) Cumulative probabilities of amplitudes of mEPSCs recorded in *Tsc1*^{wt} (n=8, N=3) (**h**) and *Tsc1*$^{+/-}$ (n=9, N=3) (**i**) mice in the absence and in the presence of 10 μM DQP1105. For pairs of cumulative probabilities shown in (**g-i**) distributions do not differ significantly (Mann-Whitney test: p>0.05). Error bars:±s.e.m. (**j,k**) Summary data for the effects of DQP1105 (10 μM) on normalized charges of mEPSC (**j**) and on weighted time constant, τ_w of mEPSC decay (**k**) in L4 in *Tsc1*^{wt} and in *Tsc1*$^{+/-}$ mice. (**l**) Summary data for the effects of DQP1105 (10 μM) on mEPSC amplitude in *Tsc1*^{wt} and in *Tsc1*$^{+/-}$ mice. All means±s.e.m., ***p<0.001. All data sets were analyzed using one-way ANOVA (see **Supplementary Table 2** for statistics).

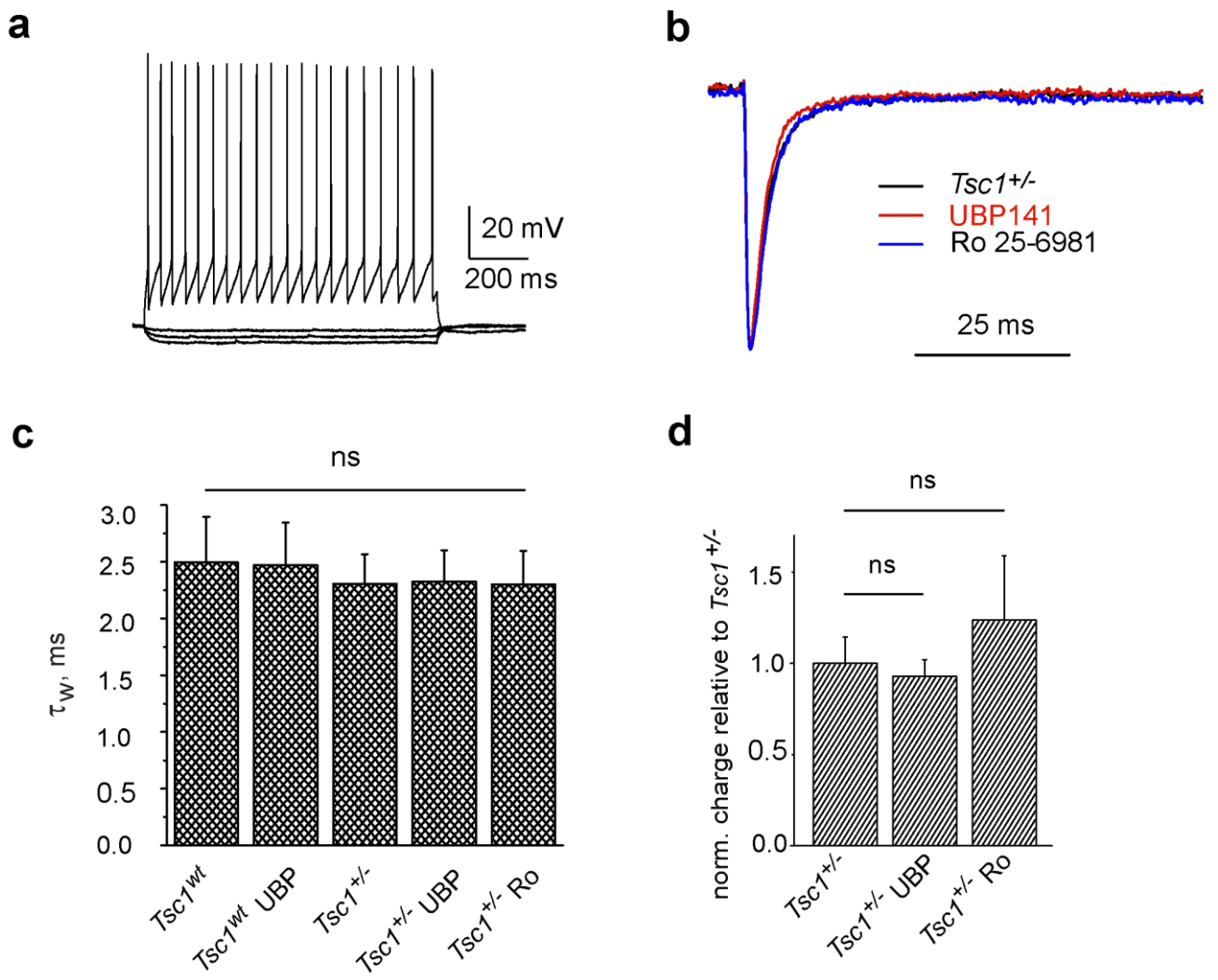

Supplementary Figure 6 **NMDARs in fast-spiking (FS) interneurons in *Tsc1*$^{+/-}$ mice are not affected by preferential GLuN2C/D (UBP141) and selective GluN2B (Ro25-6981) antagonists.** (**a**) Firing pattern of fast-spiking interneuron in response to hyperpolarizing and depolarizing current injection recorded in L4 in neocortical slices from *Tsc1*$^{+/-}$ mice. (**b**) Superimposed averaged normalized traces of sEPSC recorded at -50 mV from FS interneuron in L4 in neocortical slices from *Tsc1*$^{+/-}$ mice in control (n=9 cells, N= 4 mice), in the presence of 1 μM Ro25-6981 (n=5 cells, N=3 mice) or 10 μM UBP141 (n=5 cells, N= 3 mice). (**c,d**) Summary data for the effects of UBP141 and Ro25-6981 on weighted time constant, τ_w of sEPSC decay (**c**) and on normalized charges of sEPSC (**d**) in L4 FS interneurons. n=5 cells, N=3 mice for *Tsc1*^{wt} mice in control, and n=4, N=3 mice in the presence of UBP141. All means±s.e.m. Data were analyzed using one-way ANOVA followed by Fisher's LSD post-hoc test (see **Supplementary Table 2** for statistics).

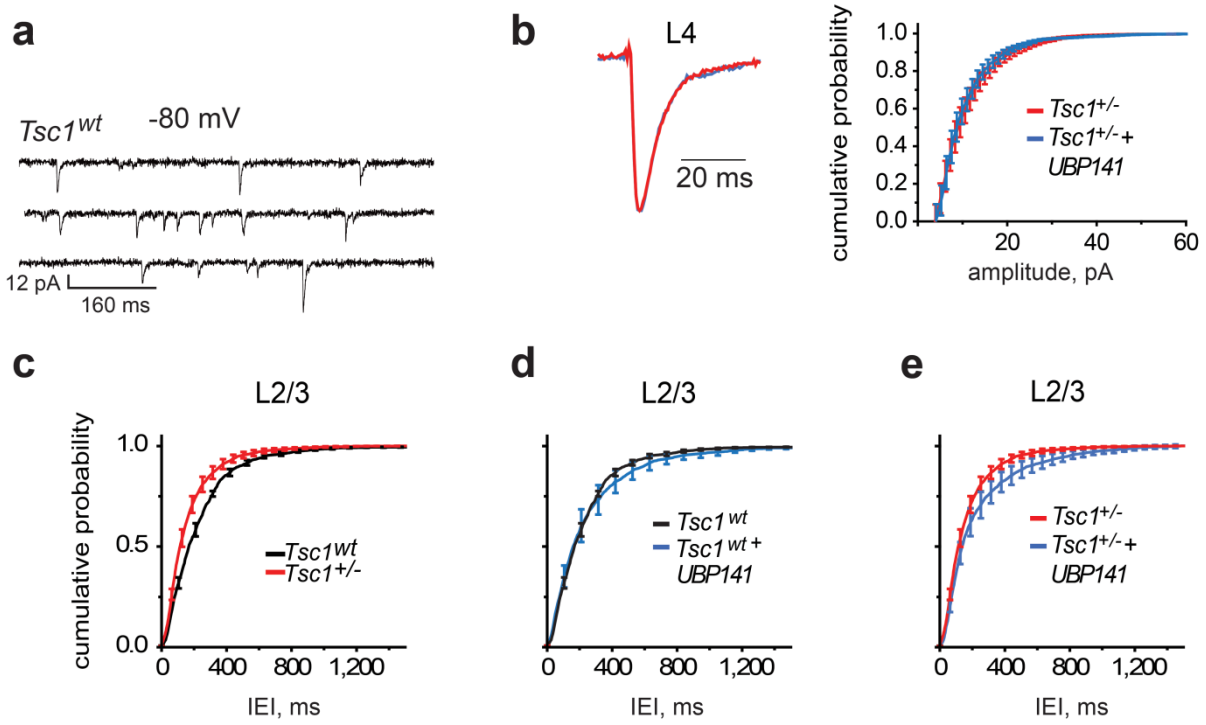

Supplementary Figure 7 Effects of UBP141 on AMPA receptor-mediated spontaneous EPSCs in layers L4 and L2/3. (**a**) Representative traces of spontaneous activity recorded in whole-cell patch-clamp mode at holding potential -80 mV in L2/3 pyramidal neurons in coronal neocortical slices from *Tsc1*^{wt} mice. (**b**) Left: Superimposed non-normalized averaged traces of sEPSC recorded in L4 spiny stellate cells *Tsc1*$^{+/-}$ mice at -80 mV in control and in the presence of 10 µM of UBP141 (n=7, N=3 mice). Note, that neither amplitude nor kinetics of AMPAR-mediated sEPCS was altered by UBP141. Right: The cumulative probabilities of amplitudes of individual sEPSCs recorded in control and in the presence of UBP141. (**c-e**) Cumulative probabilities of inter event intervals (IEI) of individual sEPSCs recorded in L2/3 in *Tsc1*^{wt} (n=10, N=3 mice) and *Tsc1*$^{+/-}$ mice (n=28, N=5 mice) in control and in *Tsc1*^{wt} (n=5, N=3 mice) and *Tsc1*$^{+/-}$ mice (n=21, N=5 mice) in the presence of UBP141. For pairs of cumulative probabilities shown in (**c**) and (**e**) distributions differ significantly (Kolmogorov-Smirnov test: $p<0.05$). Error bars:±s.e.m.

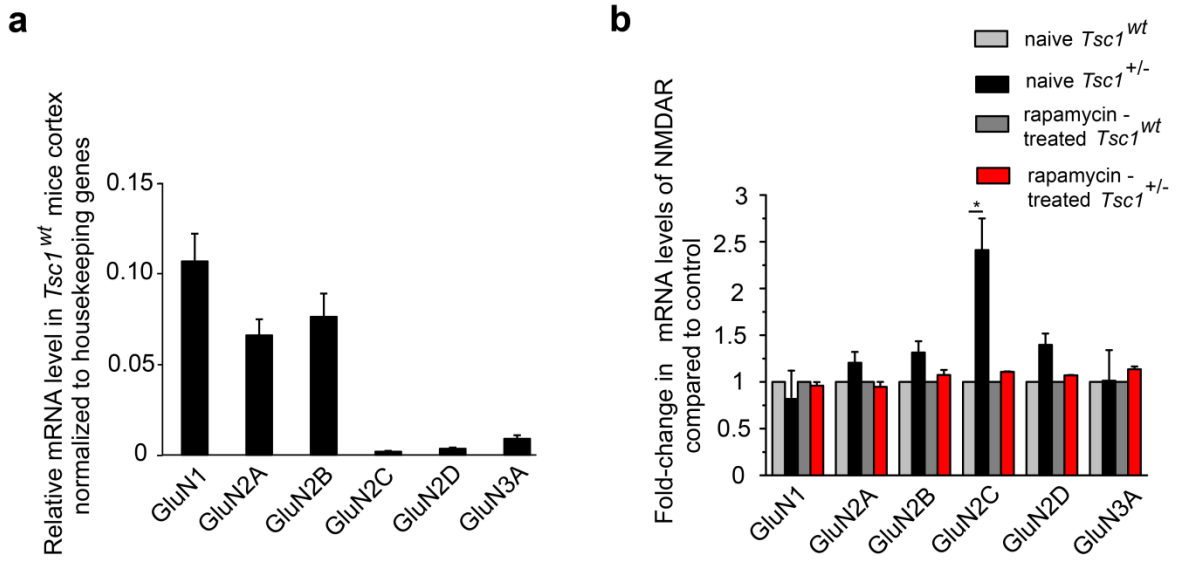

Supplementary Figure 8 Relative expression of mRNAs encoding different NMDAR subunits in the cortex of *Tsc1^{wt}* and *Tsc1$^{+/-}$* mice. (**a**) Quantitative RT-PCR showing the relative expression of mRNAs encoding different NMDAR subunits in the cerebral cortex of *Tsc1^{wt}* mice at P16. Hypoxanthine phosphoribosyltransferase 1 (HPRT) and Cyclophilin-A were used for normalization. Results are mean±s.e.m. (N=5 mice for each group). (**b**) Relative expression of mRNAs encoding NMDAR subunits in naïve *Tsc1$^{+/-}$* mice compared to naïve *Tsc1^{wt}* mice and in *Tsc1$^{+/-}$* mice compared to *Tsc1^{wt}* mice both treated with rapamycin. Note the absence of GluN2C up-regulation in rapamycin-treated *Tsc1$^{+/-}$* mice. All means±s.e.m., *p<0.05. two-tailed t-test.

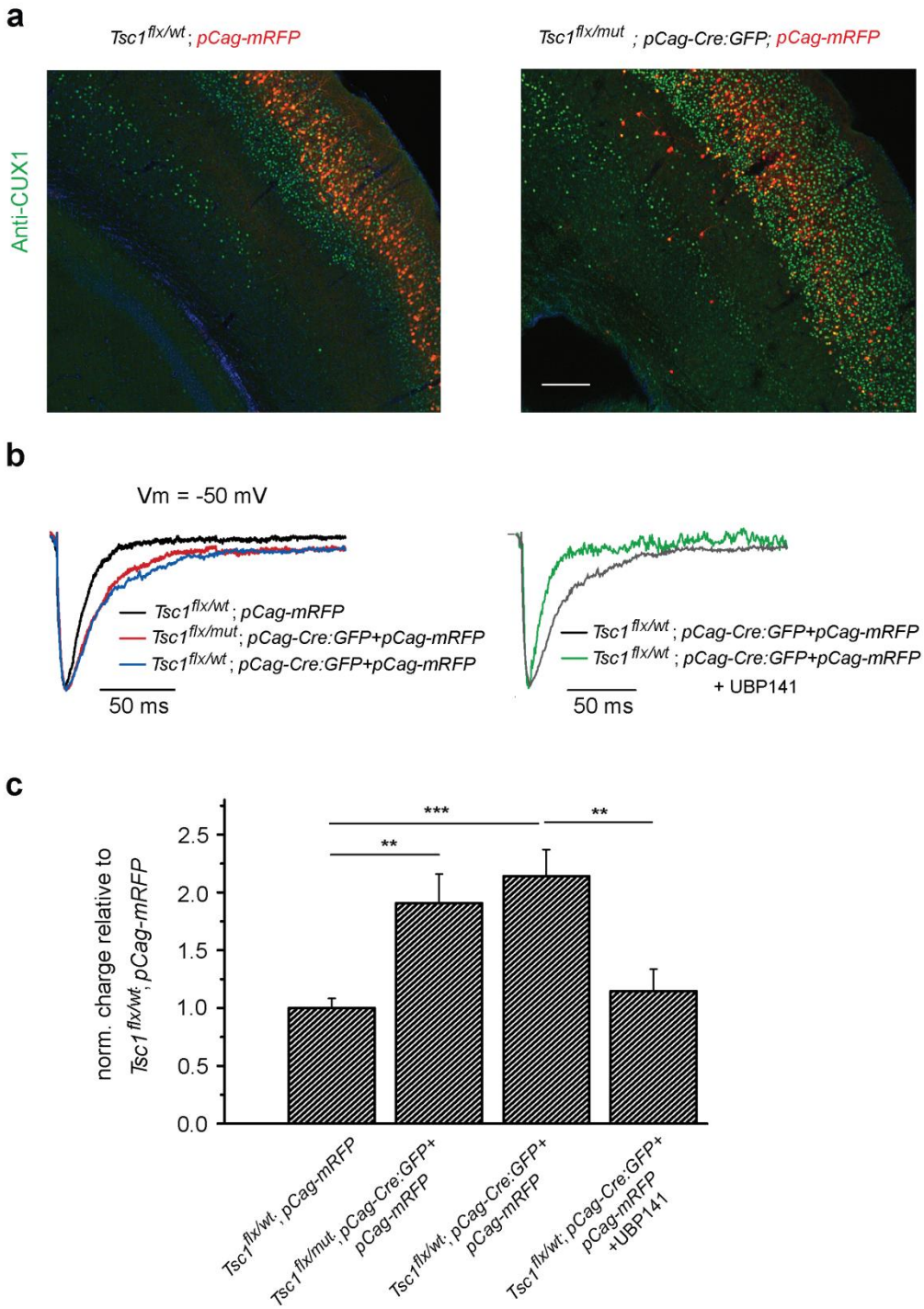

Supplementary Figure 9 Single-cell heterozygote or homozygote *Tsc1* knockout induces up-regulation of slow UBP141-sensitive component of NMDA receptor mediated synaptic transmission. (**a**) Confocal photographs of electroporated cells in neocortical slices from *Tsc1*$^{flx/wt}$ (left) and *Tsc1*$^{flx/mut}$;pCAG-Cre (right) mice expressing mRFP (red) and immunostained with CUX1 antibody (green) to label cortical layers L1-L4. Scale bar applies for both images, 200 µm. (**b**) Left: Superimposed averaged normalized traces of sEPSC recorded at -50 mV from electroporated *Tsc1*^{haplo} and *Tsc1*^{null} neurons. *Tsc1*$^{flx/wt}$ mice that were electroporated with pCAG-mRFP only have been used as controls. Right: Superimposed averaged normalized traces of sEPSC recorded at -50 mV from *Tsc1*^{haplo} neurons without and in the presence of 10 µM UBP141. (**c**) Summary data for normalized charges of sEPSC in *Tsc1*$^{flx/wt}$; pCag-mRFP (n=10 cells, N=4 mice), *Tsc1*$^{flx/mut}$;pCAG-Cre (n=6 cells, N=3 mice), *Tsc1*$^{flx/wt}$;pCAG-Cre (n=13 cells, N=5 mice) and in *Tsc1*$^{flx/wt}$;pCAG-Cre mice in the presence of UBP141 (n=4 cells, N=3 mice). All means±s.e.m., *p<0.05, **p<0.01, ***p<0.001. Data were analyzed using one-way ANOVA followed by Fisher's LSD post-hoc test (see **Supplementary Table 2** for statistics).

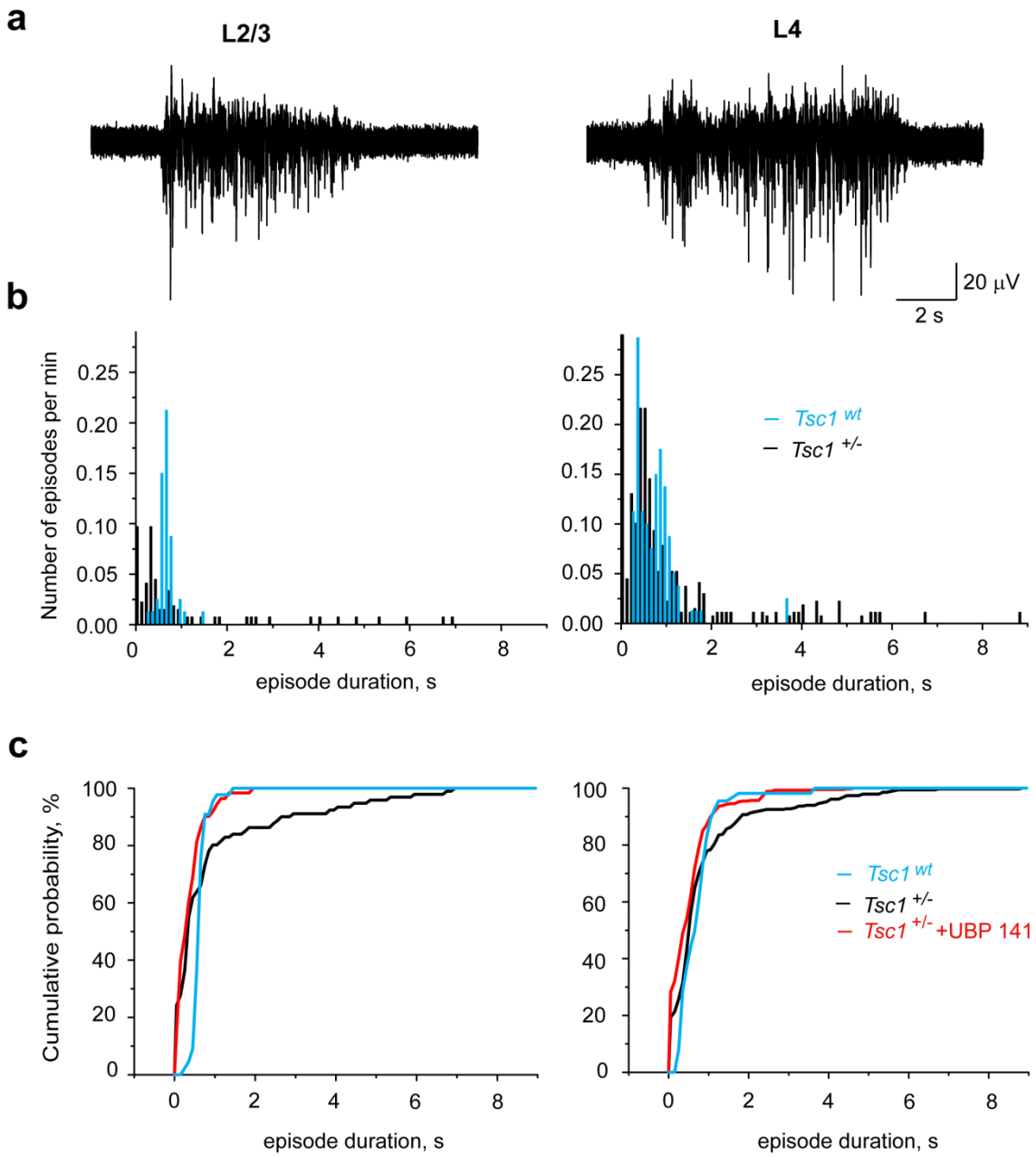

Supplementary Figure 10 Field extracellular recordings of spontaneous epileptiform activity in neocortical slices of *Tsc1*$^{+/-}$ mice. (**a**) Representative traces of seizure-like activity recorded from two channels of multichannel array recording system in L2/3 (left) and L4 (right) in neocortical slices from *Tsc1*$^{+/-}$ mice. (**b**) Distribution of high-amplitude episode durations in L2/3 (left) and L4 (right) of *Tsc1*^{wt} (blue) and *Tsc1*$^{+/-}$ (black) mice. *Tsc1*^{wt} (L2/3): n=52 episodes, N=3 mice; *Tsc1*^{wt} (L4): n=179 episodes, N=3 mice; *Tsc1*$^{+/-}$ (L2/3): n=66 episodes, N=3 mice; *Tsc1*$^{+/-}$ (L4): n=218 episodes, N=3 mice; (**c**) Cumulative probability of the high-amplitude episodes duration without (black) and with 10 μM UBP141 in bath (red) in L2/3 (left) and L4 (right) in *Tsc1*$^{+/-}$ mice. Respective cumulative probabilities for *Tsc1*^{wt} mice are shown in blue. *Tsc1*^{wt} (L2/3): n=52 episodes, N=3 mice; *Tsc1*^{wt} (L4): n=179 episodes, N=3 mice; *Tsc1*$^{+/-}$ (L2/3): n=66 episodes, N=3 mice; *Tsc1*$^{+/-}$ (L2/3, UBP141); n=50, N=3; *Tsc1*$^{+/-}$ (L4): n=218 episodes, N=3 mice; *Tsc1*$^{+/-}$ (L4, UBP141); n=200 episodes, N=3 mice.
Distributions for *Tsc1*^{wt} and *Tsc1*$^{+/-}$ differ significantly for both layers (Kolmogorov-Smirnov test: $p<0.05$). Distributions for *Tsc1*$^{+/-}$ without and with UBP141 differ significantly for both layers (Kolmogorov-Smirnov test: $p<0.05$).

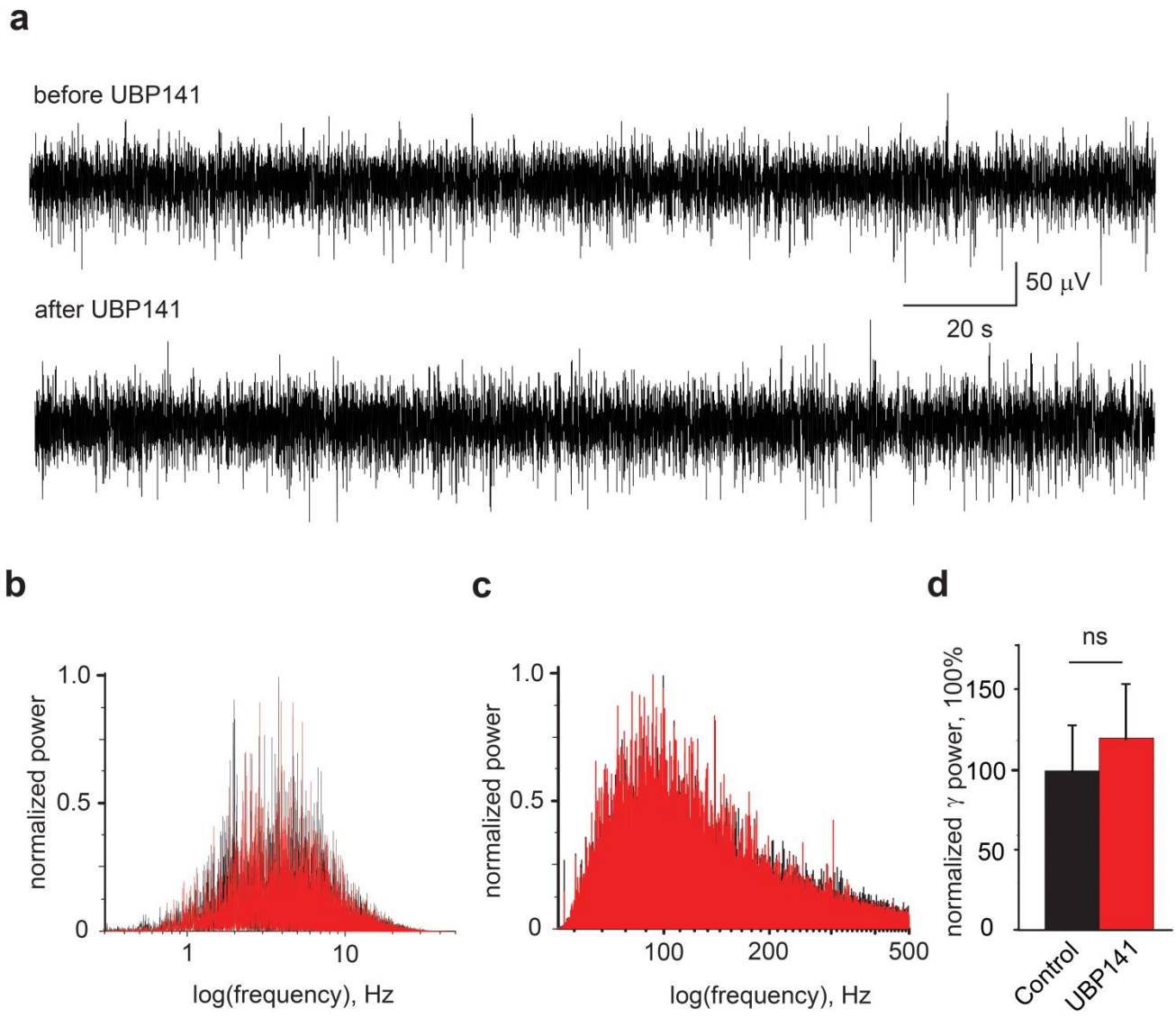

Supplementary Figure 11 Basal (interseizure) activity in *Tsc1*$^{+/-}$ mice is not altered after UBP141 (75 mg kg^{-1}) injection *in vivo.* (**a**) Representative traces of basal activity in L4 before (upper trace) and 40 min after UBP141 IP injection (lower trace). (**b, c**) Corresponding spectral Fast Fourier Transform (FFT) histogram of normalized power of basal activity with (red) and without (black) UBP141 in L4 (10 min recordings for each condition were analyzed) at frequencies <50 Hz (**b**) and >50 Hz (**c**). (**d**) Normalized integral power of γ-band components of basal activity in L4 without (control) and with UBP141 (N=5 mice, p>0.3, two-tailed t-test). All means±s.e.m.

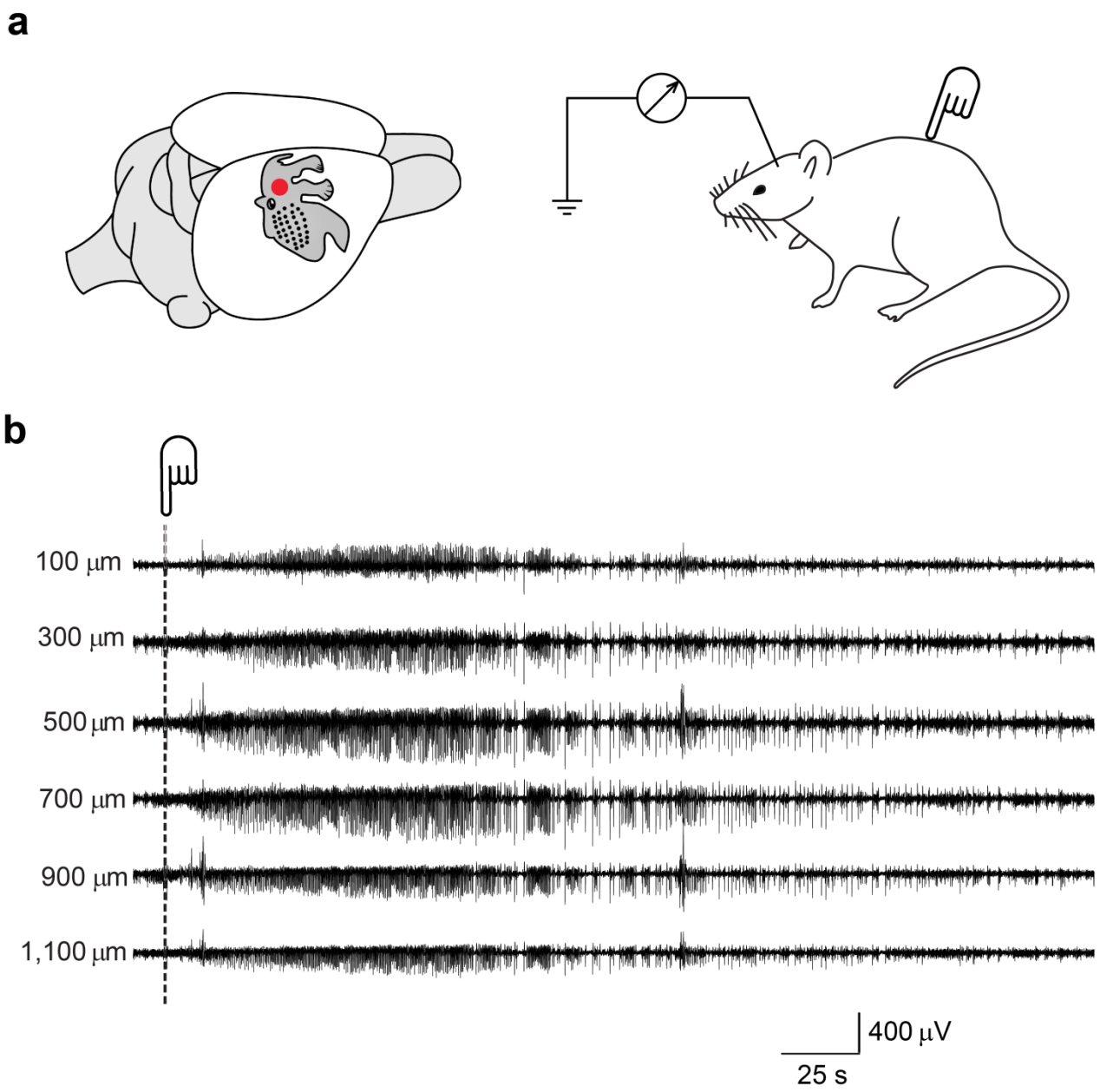

Supplementary Figure 12 Tactile stimulation of sensory inputs to L4 induces generalized seizures in *Tsc1*$^{+/-}$ mice *in vivo.* (**a**) Left: Schematic showing representation of the body surface in mouse somatosensory cortex. Sensory information from the body surfaces is projected through ascending pathways and represented in a somatotopic map in the somatosensory cortex. Right: Experimental setup. (**b**) Representative electrographic seizures in neocortex induced by tactile stimulus at the time point indicated by dashed line. Shown are epileptic discharges recorded at the depth indicated on the left of each trace.

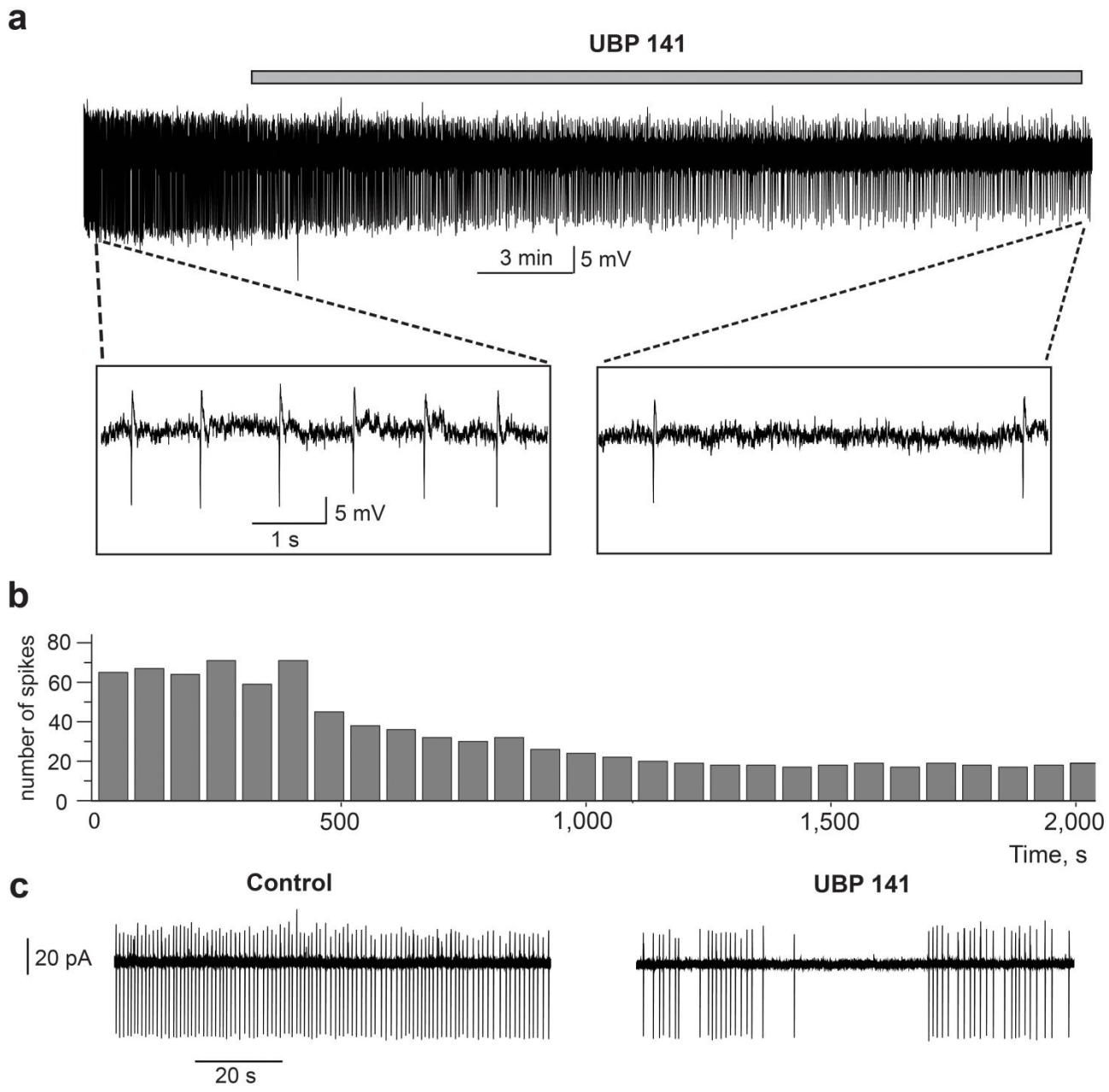

Supplementary Figure 13 Selective GluN2C/D antagonist UBP141 reduces spontaneous paroxysmal hyperexcitability in human postsurgical tissue of TSC patients. (**a**) Field potential extracellular recording of spontaneous paroxysmal activity in neocortical slice**.** Insets show spikes in extended time scale. Note that application of UBP141 (10 μM) reduces frequency of spontaneous spiking. (**b**) Corresponding time course of the UBP141-induced firing frequency change. (**c**) Representative traces of a single cell spontaneous paroxysmal activity recorded in cell-attached mode from dysplastic cell in a neocortical slice in control (left) and in the presence of 10 μM UBP141 in the bath (right). In (**a**) and (**c**) data were obtained from samples from two different TSC patients.

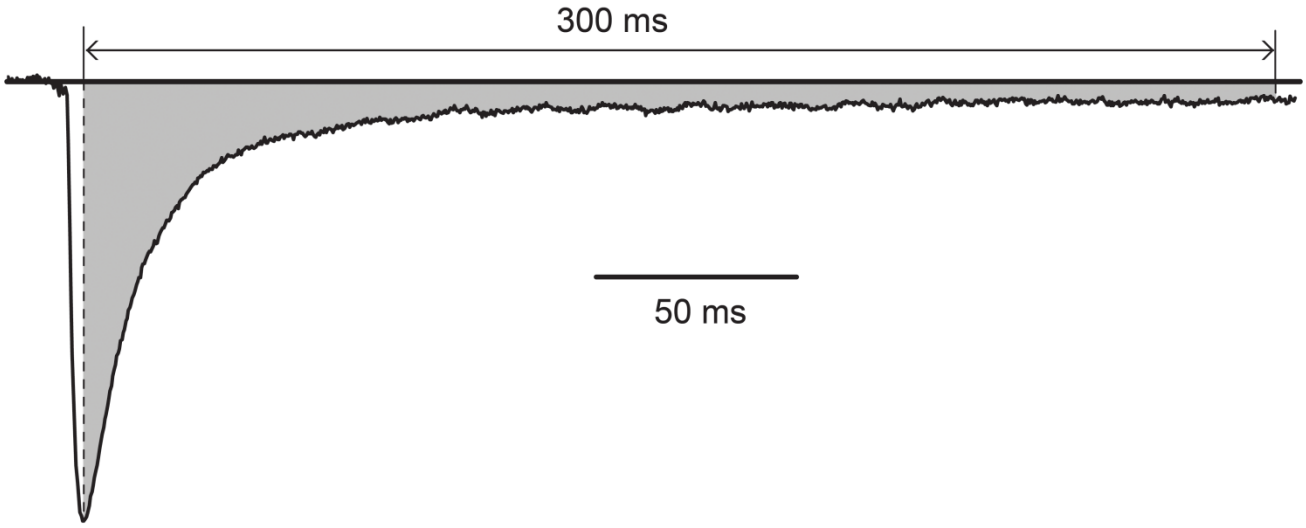

Supplementary Figure 14 Charge transfer calculation. Example EPSC trace. Charge transfer was calculated by the integrating the area shown in gray under the current waveform in the interval of time between peak of sEPSC and 300 ms after the peak.

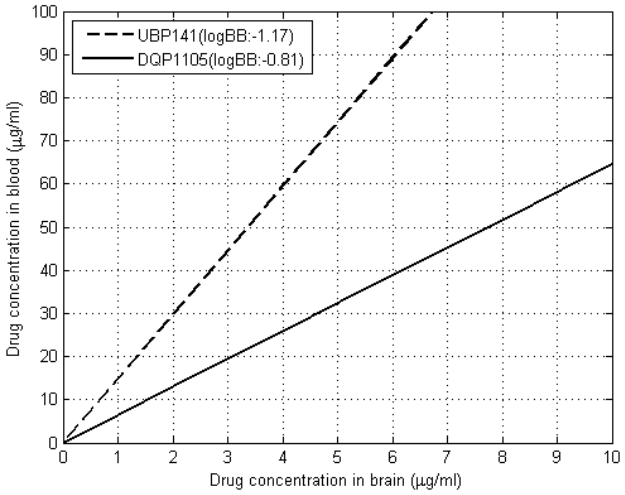

Supplementary Figure 15 Brain and blood concentration relationships for the UBP141 and DQP1105 substances. Brain and blood concentration relationships for the UBP141 and DQP1105 substances devised from the decimal logarithm of brain to plasma concentration ratio (logBB) based mainly on the passive transport (diffusion). The logBB parameter is described as linear cumulative distribution function.

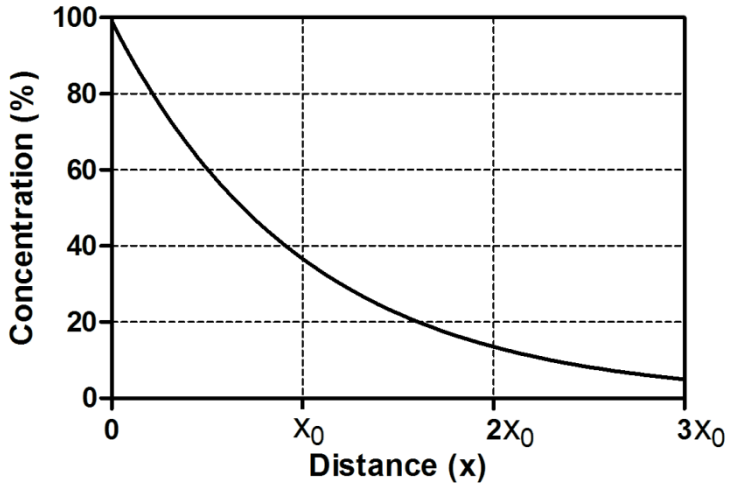

Supplementary Figure 16 Conceptual diagram of drug concentration kinetics in tissue adjacent to the peritoneal cavity. Initial point (100%) is a free drug concentration in the peritoneal fluid. Solid line shows the exponential decrease in the free tissue interstitial concentration (in capillary bed) of reference drug. The concentration reduction depends on the distance (x) from the serosal surface. x_0 - characteristic diffusion length (average distance traveled by drug molecules), at which the concentration difference between the peritoneal fluid and the blood decreases to 37% of its maximum value.

Supplementary Table 1

NMDAR antagonists selectivity at recombinant NMDAR receptors

	IC_{50} (μM)								
	GluN2A	**GluN2B**	**GluN2C**	**GluN2D**	**GluA1**	**GluK2**	**refs**	***In vitro* concentration (present study)**	***In vivo* IP injection dosage (present study)**
Ro25-6981 Selective antagonist of GluN2B	52	0.009					[1]	1 μM	
UBP141 Preferential competitive antagonist of GluN2C/D	22	17.2	5.24	2.36	>100	>100	[2]	10 μM	75mg kg^{-1}
DQP1105 Selective noncompetitive antagonist of GluN2C/D	206	121	8.5	2.7	198	153	[3]	10 μM	28mg kg^{-1}

Supplementary Table 2

ANOVA statistical analysis

Figure 3 (e-j)	*Number of mice tested*
L2/3- Tsc1^{wt}	5
L2/3- Tsc1^{wt}-UBP	**3**
L2/3- Tsc1^{wt}-Ro	**3**
L2/3- Tsc1$^{+/-}$	**8**
L2/3- Tsc1$^{+/-}$ -UBP	**4**
L2/3-Tsc1$^{+/-}$ -Ro	**3**
L4- Tsc1^{wt}	6
L4- Tsc1^{wt}-UBP	**3**
L4- Tsc1^{wt}-DQP	**3**
L4- Tsc1^{wt}-Ro	**3**
L4- Tsc1$^{+/-}$	**10**
L4- Tsc1$^{+/-}$ -UBP	**5**
L4- Tsc1$^{+/-}$ -DQP	**3**
L4-Tsc1$^{+/-}$ -Ro	**3**
L4-Tsc1^{wt} -vehicle	**3**
L4-Tsc1^{wt} -vehicle -UBP	**3**
L4-Tsc1$^{+/-}$ -vehicle	**3**
L4-Tsc1$^{+/-}$ -vehicle -UBP	**3**
L4-Tsc1$^{+/-}$ -Rapamycin	**3**
L4-Tsc1$^{+/-}$-Rapamycin-UBP	**3**

Figure 3e	*N1*	*N2*	*Univariate ANOVA between the groups*	*Post-hoc test between the groups Fisher test (p values)*
L2/3- Tsc1^{wt}-UBP L2/3-Tsc1^{wt}	9	16	2.40*E-4	0.49
L2/3- Tsc1^{wt}-Ro L2/3-Tsc1^{wt}	6	16		0.48
L2/3-Tsc1$^{+/-}$ L2/3-Tsc1^{wt}	27	16		7.82E-05 (*)
L2/3-Tsc1$^{+/-}$ -UBP L2/3- Tsc1$^{+/-}$	12	27		0.017 (*)
L2/3-Tsc1$^{+/-}$ -Ro L2/3- Tsc1$^{+/-}$	9	27		0.004 (*)

Figure 3f			*Univariate ANOVA between the groups*	*Post-hoc test between the groups Fisher test (p values)*
L4-Tsc1^{wt}-UBP L4-Tsc1^{wt}	9	29	3.44*E-13	0.82
L4-Tsc1^{wt}-Ro L4-Tsc1^{wt}	4	29		0.71
L4- Tsc1^{wt}-DQP L4-Tsc1^{wt}	12	29		0.98
L4-Tsc1$^{+/-}$ L4-Tsc1^{wt}	34	29		5.6*E-18 (*)
L4-Tsc1$^{+/-}$ -UBP L4-Tsc1$^{+/-}$	10	34		3.4*E-08 (*)

L4-Tsc1$^{+/-}$-Ro L4-Tsc1$^{+/-}$	12	34		0.08
L4-Tsc1$^{+/-}$-DQP L4-Tsc1$^{+/-}$	12	34		1.1E-09 (*)

Figure 3g			*Univariate ANOVA between the groups*	*Post-hoc test between the groups Fisher test (p values)*
L4-Tsc1^{wt}-vehicle -UBP L4-Tsc1^{wt} -vehicle	8	12		0.66
L4-Tsc1$^{+/-}$-vehicle L4-Tsc1^{wt} -vehicle	11	12		5.56*E-14 (*)
L4-Tsc1$^{+/-}$-vehicle -UBP L4-Tsc1$^{+/-}$ -vehicle	7	11		6.8*E-08 (*)
L4-Tsc1$^{+/-}$-Rapamycin L4-Tsc1^{wt} -vehicle	14	12		0.67
L4-Tsc1$^{+/-}$-Rapamycin L4-Tsc1$^{+/-}$ -vehicle	14	11		6.77*E-14 (*)
L4-Tsc1$^{+/-}$-Rapamycin-UBP L4-Tsc1$^{+/-}$ -Rapamycin	11	14	1.87*E-14	0.78

Figure 3h	*N1*	*N2*	*Univariate ANOVA between the groups*	*Post-hoc test between the groups Fisher test (p values)*
L2/3- Tsc1^{wt}-UBP L2/3-Tsc1^{wt}	9	16		0.73
L2/3- Tsc1^{wt}-Ro L2/3-Tsc1^{wt}	6	16		0.84
L2/3-Tsc1$^{+/-}$ L2/3-Tsc1^{wt}	27	16		6*E-7(*)
L2/3-Tsc1$^{+/-}$-UBP L2/3- Tsc1$^{+/-}$	14	27		5*E-4 (*)
L2/3-Tsc1$^{+/-}$-Ro L2/3- Tsc1$^{+/-}$	9	27	1.63*E-6	0.002 (*)

Figure 3i			*Univariate ANOVA between the groups*	*Post-hoc test between the groups Fisher test (p values)*
L4-Tsc1^{wt}-UBP L4-Tsc1^{wt}	10	27		0.77
L4-Tsc1^{wt}-Ro L4-Tsc1^{wt}	4	27		0.93
L4- Tsc1^{wt}-DQP L4-Tsc1^{wt}	12	27		0.79
L4-Tsc1$^{+/-}$ L4-Tsc1^{wt}	33	27		2.26*E-12 (*)
L4-Tsc1$^{+/-}$-UBP L4-Tsc1$^{+/-}$	10	33		5.75*E-9 (*)
L4-Tsc1$^{+/-}$-Ro L4-Tsc1$^{+/-}$	12	33		0.23
L4-Tsc1$^{+/-}$-DQP L4-Tsc1$^{+/-}$	12	33	1.5*E-14	3*E-9 (*)

Figure 3j			*Univariate ANOVA between the groups*	*Post-hoc test between the groups Fisher test (p values)*
L4-Tsc1^{wt}-vehicle -UBP L4-Tsc1^{wt} -vehicle	10	13		0.44
L4-Tsc1$^{+/-}$-vehicle L4-Tsc1^{wt} -vehicle	9	13		2*E-14 (*)
L4-Tsc1$^{+/-}$-vehicle -UBP L4-Tsc1$^{+/-}$ -vehicle	8	9	5.5*E-16	1*E-10 (*)

L4-Tsc1$^{+/-}$-Rapamycin *L4-Tsc1^{wt} -vehicle*	14	13		0.18
L4-Tsc1$^{+/-}$-Rapamycin *L4-Tsc1$^{+/-}$ -vehicle*	14	9		2*E-16 (*)
L4-Tsc1$^{+/-}$-Rapamycin-UBP *L4-Tsc1$^{+/-}$ -Rapamycin*	13	14		0.81

Supplementary Figure 4j	*N1*	*N2*	*Univariate ANOVA between the groups (p values)*
L2/3- Tsc1^{wt}-UBP *L2/3-Tsc1^{wt}*	9	16	
L2/3- Tsc1^{wt}-Ro *L2/3-Tsc1^{wt}*	6	16	
L2/3-Tsc1$^{+/-}$ *L2/3-Tsc1^{wt}*	27	16	
L2/3-Tsc1$^{+/-}$-UBP *L2/3- Tsc1$^{+/-}$*	13	27	
L2/3-Tsc1$^{+/-}$-Ro *L2/3- Tsc1$^{+/-}$*	9	27	0.14575

Supplementary Figure 4k			*Univariate ANOVA between the groups (p values)*
L4-Tsc1^{wt}-UBP *L4-Tsc1^{wt}*	9	28	
L4-Tsc1^{wt}-Ro *L4-Tsc1^{wt}*	4	28	
L4- Tsc1^{wt}-DQP *L4-Tsc1^{wt}*	12	28	
L4-Tsc1$^{+/-}$ *L4-Tsc1^{wt}*	34	28	
L4-Tsc1$^{+/-}$-UBP *L4-Tsc1$^{+/-}$*	10	34	
L4-Tsc1$^{+/-}$-Ro *L4-Tsc1$^{+/-}$*	12	34	
L4-Tsc1$^{+/-}$-DQP *L4-Tsc1$^{+/-}$*	12	34	0.97839

Supplementary Figure 4l			*Univariate ANOVA between the groups (p values)*
L4-Tsc1^{wt}-vehicle -UBP *L4-Tsc1^{wt} -vehicle*	9	12	
L4-Tsc1$^{+/-}$-vehicle *L4-Tsc1^{wt} -vehicle*	11	12	
L4-Tsc1$^{+/-}$-vehicle -UBP *L4-Tsc1$^{+/-}$ -vehicle*	8	11	
L4-Tsc1$^{+/-}$-Rapamycin *L4-Tsc1^{wt} -vehicle*	14	12	
L4-Tsc1$^{+/-}$-Rapamycin *L4-Tsc1$^{+/-}$ -vehicle*	14	11	
L4-Tsc1$^{+/-}$-Rapamycin *L4-Tsc1$^{+/-}$ -vehicle-UBP*	14	8	
L4-Tsc1$^{+/-}$-Rapamycin-UBP *L4-Tsc1$^{+/-}$ -vehicle*	8	11	
L4-Tsc1$^{+/-}$-Rapamycin-UBP *L4-Tsc1$^{+/-}$ -Rapamycin*	8	14	0.4127

Supplementary Figure 5j			*Univariate ANOVA between the groups*	*Post-hoc test between the groups Fisher test (p values)*

L4- Tsc1^{wt}-DQP L4-Tsc1^{wt}	7	9		0.90138
L4-Tsc1$^{+/-}$ L4-Tsc1^{wt}	10	9		2.41*E-08(*)
L4-Tsc1$^{+/-}$-DQP L4-Tsc1$^{+/-}$	8	10	1.38*E-08	3.11*E-07 (*)

Supplementary Figure 5k			*Univariate ANOVA between the groups*	*Post-hoc test between the groups Fisher test (p values)*
L4- Tsc1^{wt}-DQP L4-Tsc1^{wt}	8	9		0.35712
L4-Tsc1$^{+/-}$ L4-Tsc1^{wt}	10	9		3.52*E-12(*)
L4-Tsc1$^{+/-}$-DQP L4-Tsc1$^{+/-}$	9	10	3.5*E-12	4.33*E-10 (*)

Supplementary Figure 5l			*Univariate ANOVA between the groups (p values)*
L4- Tsc1^{wt}-DQP L4-Tsc1^{wt}	8	8	
L4-Tsc1$^{+/-}$ L4-Tsc1^{wt}	10	8	
L4-Tsc1$^{+/-}$-DQP L4-Tsc1$^{+/-}$	9	10	0.87445

Supplementary Figure 6c	*N1*	*N2*	*Univariate ANOVA between the groups (p values)*
L4- Tsc1^{wt}-interneuron-UBP L4-Tsc1^{wt} interneuron	4	5	
L4-Tsc1^{wt} interneuron L4-Tsc1$^{+/-}$-interneuron	5	9	
L4-Tsc1$^{+/-}$-interneuron -UBP L4-Tsc1$^{+/-}$-interneuron	5	9	
L4-Tsc1$^{+/-}$-interneuron -Ro L4-Tsc1$^{+/-}$-interneuron	5	9	0.98

Supplementary Figure 6d			*Univariate ANOVA between the groups (p values)*
L4-Tsc1$^{+/-}$-interneuron -UBP L4-Tsc1$^{+/-}$-interneuron	5	9	
L4-Tsc1$^{+/-}$-interneuron -Ro L4-Tsc1$^{+/-}$-interneuron	5	9	0.61

Supplementary Figure 9c			*Univariate ANOVA between the groups*	*Post-hoc test between the groups Fisher test (p values)*
Tsc1$^{flx/mut}$;pCAG-Cre:GFP Tsc1$^{flx/wt}$;pCAG-mRFP	6	10	7.29*E-04	0.008 (*)

Tsc1$^{flx/wt}$;*pCAG-Cre:GFP* *Tsc1*$^{flx/wt}$;*pCAG-mRFP*	13	10		1.54E-04 (*)
Tsc1$^{flx/wt}$;*pCAG-Cre:GFP* *Tsc1*$^{flx/mut}$;*pCAG-Cre:GFP*	13	6		0.45
Tsc1$^{flx/mut}$;*pCAG-Cre:GFP-UBP* *Tsc1*$^{flx/mut}$;*pCAG-Cre:GFP*	4	13		0.0091 (*)

Supplementary Table 3

Clinical features of TSC samples collected following epilepsy surgery

Number	1	2	3
Sex	M	F	M
Mutated gene	*TSC2*	*TSC2*	*TSC2*
Onset of seizures	4 days	Birth	2 months
Type of seizures	Partial left occipital	Partial left-side clonic	Partial right frontal
Age at surgery	8 months	16 months	7 months
Type of surgery	Left parieto-occipital resection	Left occipito-temporal resection	Right frontal resection
Histology of lesion	Dysplasia 2B	Tuber	Tuber
AEDs at surgery	VGB,TPM,CBZ	VGB	VGB, CBZ, TPM
AEDs after surgery	VGB,TPM, CBZ, PHB,CZP	VGB, LVT, CBZ	VGB, CBZ, TPM

AEDs, antiepileptic drugs
TSC2 – Tuberous sclerosis 2
VGB – Vigabatrin
TPM – Topiramate
CBZ – Carbamazepine
LVT – Levetiracetam
CZP – Clonazepam
PHB – Phenobarbital

Supplementary Table 4

Clinical features of focal cortical dysplasia samples collected following epilepsy surgery

Number	1	2	3	4	5
Sex	F	M	F	F	F
Mutated gene	*TSC2 de novo*	*NA*	*NA*	*NA*	*NA*
Onset of seizures	5 months	20 months	6 1/2 years	20 months	9 years
Type of seizures (according to EEG)	Generalized clonic, partial clonic	Partial right frontal	Partial right temporal	Partial left frontal	Complex partial right temporal
Age at surgery	13 months	5 years	6 1/2 years	4 1/2 years	11 1/2 years
Type of surgery	Resection of left ventricular SEGA and tuber when accessing to SEGA	Right frontal resection	Right parieto-temporal resection	Left frontal resection	Right temporal resection including hippocampus
Histology of lesion	FCD 2b, tuber	FCD 2b	FCD 2b	FCD 2b	FCD 2a + HS
AEDs at surgery	VGB	LVT, VGB	TPM, LVT, LTG	TPM, CBZ	OXC, LVT, LCS
AEDs after surgery	VGB	LVT, VPA	LCS, LVT, LTG	TPM, CBZ	OXC

AEDs - Antiepileptic drugs
VGB - Vigabatrin
VPA - Valproate
TPM - Topiramate
LCS - Locasamide
OXC - Oxcarbazepine
LVT - Levetiracetam
CBZ - Carbamazepine
LTG - Lamotrigine
HS - Hippocampal sclerosis

Supplementary Table 5

Human and mouse primer sequences for real time RT-PCR.

mouse		
Gene	**NCBI accession number**	**Sequences 5'->3'**
TSC1	NM_022887.3	acagctgagggggaggag
		gatggtacatcagtttccagtgc
TSC2	NM_011647.2, NM_001039363.1	tggcaaaaactaagaagcttgag
		gctctggctgtagcaagtctg
Grin2A	NM_008170.2	ctgaataaggaccgggaatg
		aatgctgaggtggttgtcatc
Grin2B	NM_008171.3	tgctgtagctgtctttgtctttg
		ctttgccgatggtgaaagat
Grin2C	NM_010350.2	gaggttctgctgtggtcctc
		attcctccagcaccttgaac
Grin3A	NM_001033351.1	gcctttctacatacacagcgaac
		accttgagaaggatgatgaagc
Grin2D	NM_008172.2	gccctgctgcgagactat
		ctcggttatcccaggtgatg
Grin1	NM_008169.1	catttagggctatcacctcca
		cactgtgtctttttggttttgc
control PPIA	NM_008907	QT00247709 (provided by Qiagen, Germany)
control HPRT	NM_013556	QT00166768 (provided by Qiagen, Germany)

Human		
Gene	**NCBI accession number**	**Sequences 5'->3'**
TSC1	NM_001162426.1, NM_001162427.1, NM_000368.4	ctgatacagcagggagcagac
		tccagtcgacagacttgctg
TSC2	NM_000548.3, NM_001077183.1, NM_001114382.1	catcgaacggctccttca
		aacaggtcatggacgatgg
Grin2A	NM_000833.3, NM_001134408.1, NM_001134407.1	ttgcttcagtttgtgggtga
		gttgtggcagatcccagtg
Grin2B	NM_000834.3	aggagaggaagtgggaaagg
		ggtcacaatgctcagatggtc
Grin2C	NM_000835.3	actcggtgcccaactcat
		ccgctgaagcagctgtagat
Grin3A	NM_133445.2	tgctgactgcaaacttctcac
		aggccaatgccgtatcct
Grin2D	NM_000836.2	tcttcgccgtcatcttcct
		ctggggcctctggaactt
Grin1	NM_021569.2, NM_007327.2, NM_000832.5	tacaagcggcacaaggatg
		cactgtgtctttttggttttgc
control gapdh	NM_001256799.1, NM_002046.4	tccactggcgtcttcacc
		ggcagagatgatgacccttttt
control actb	NM_001101.3	ccaaccgcgagaagatga
		ccagaggcgtacagggatag

Supplementary Table 6

Predicted molecular descriptors for the analyzed compounds.

Compound	ClogP	PSA(Å^2)	logBB
UBP141	1.79	106.71	-1.17
DQP1105	3.41	99.11	-0.81

logBB - decimal logarithm of brain to blood concentration ratio
ClogP - octanol-water partitioning coefficient;
PSA - polar surface area

Supplementary References:

1. Costa, B.M. et al. N-methyl-D-aspartate (NMDA) receptor NR2 subunit selectivity of a series of novel piperazine-2,3-dicarboxylate derivatives: preferential blockade of extrasynaptic NMDA receptors in the rat hippocampal CA3-CA1 synapse. *J Pharmacol Exp Ther* **331**, 618-26 (2009).

2. Acker, T.M. et al. Mechanism for noncompetitive inhibition by novel GluN2C/D N-methyl-D-aspartate receptor subunit-selective modulators. *Mol Pharmacol* **80**, 782-95 (2011).

3. Fischer, G. et al. Ro 25-6981, a highly potent and selective blocker of N-methyl-D-aspartate receptors containing the NR2B subunit. Characterization in vitro. *J Pharmacol Exp Ther* **283,** 1285-92 (1997).